AIAA JOURNAL
Vol. 32, No. 6, June 1994

Equivalent Plate Structural Modeling for Wing Shape Optimization Including Transverse Shear

Eli Livne*
University of Washington, Seattle, Washington 98195

A new technique for structural modeling of airplane wings is presented taking transverse shear effects into account. The kinematic assumptions of first-order shear deformation plate theory in combination with numerical analysis, where simple polynomials are used to define geometry, construction, and displacement approximations, lead to analytical expressions for elements of the stiffness and mass matrices and load vector. Contributions from the cover skins, spar and rib caps, and spar and rib webs are included as well as concentrated springs and concentrated masses. Limitations of wing modeling techniques based on classical plate theory are discussed, and the improved accuracy of the new equivalent plate technique is demonstrated through comparison with finite element analysis and test results. Expressions for analytical derivatives of stiffness, mass, and load terms with respect to wing shape are given. Based on these, it is possible to obtain analytic sensitivities of displacements, stresses, and natural frequencies with respect to planform shape and depth distribution. This makes the new capability an effective structural tool for wing shape optimization.

Nomenclature

$A(y)$ = spar cap cross-sectional area
A_1^{sp}, A_2^{sp} = coefficients of spar cap area series
A_1, A_2 = coefficients of aft line of a trapezoid
$\{a_i\}$ = vectors containing polynomial terms used as Ritz functions $(n_q \times 1)$, $i = 1, 5$
B_1, B_2 = coefficients of a straight line in x, y
$c\Lambda$ = cos Λ
E = Young's modulus for spar caps
F_1, F_2 = coefficients of forward line of a trapezoid
H_{ih}^L, H_{ih}^U = coefficients in the polynomial series for $h_L, h_U(x, y)$
$h_L, h_U(x, y)$ = z coordinates of lower and upper wing surfaces
$I_F(m, n)$ = family of spar line integrals of polynomial terms
$I_{TR}(m, n)$ = family of area integrals of $x^m y^n$
i_l = index for layers on a skin trapezoid
$[K]$ = stiffness matrix
KE = kinetic energy
L_s = length of a spar
$[M]$ = mass matrix
m, n = powers of x and y in polynomial terms
n_q = number of terms in the polynomial series for one deformation field $\{q_i\}$
$p(x, y)$ = pressure load in the z direction
$\{q\}$ = vector of all generalized displacements $(5n_q \times 1)$
$\{q_i\}$ = generalized displacements for the five deformation fields, Eqs. (9), $(n_q \times 1)$, $i = 1, 5$
$[Q^{il}]$ = material constitutive matrix (3×3) for the ilth skin layer
$[\bar{Q}^{jl}]$ = material constitutive matrix for the jlth layer of spar web
$[Q^{sp}]$ = equivalent material matrix for spar cap
$[R_0(x, y)], [R_1(x, y)]$ = matrices containing polynomial terms in x and y, Eqs. (12) and (14), $(3 \times 5n_q)$
$[S_0(x, y)], [S_1(x, y)]$ = matrices containing polynomial terms in x and y, Eqs. (19) and (20), $(3 \times 5n_q)$
S_1^P, S_2^P = spar line coefficients
$s\Lambda$ = sin Λ
T_{25} = geometric transformation matrix for web in-plane strains
$t^{jl}(\eta, z)$ = thickness distribution of jlth layer in the spar web
$t^{il}(x, y)$ = thickness distribution of the ilth layer of the skin
U = strain energy
u, v, w = x, y, and z components of displacement
u_0, v_0, w_0 = x, y, and z components of displacement at $z = 0$
$[W_0(x, y)], [W_1(x, y)]$ = matrices containing polynomial terms, Eqs. (45) and (46), $(5 \times 5n_q)$
$[W(x, y, z)]$ = matrix expressing strains $\{\bar{\varepsilon}\}$ in terms of the generalized displacements $(5 \times 5n_q)$
$x_F(y), x_A(y)$ = x coordinates of points on the leading edge and trailing edge of an area trapezoid
$y_L, y_R, x_{FL}, x_{AR}, x_{AL}, x_{AR}$ = coordinates of vertices of an area trapezoid
y_L, y_R, x_L, x_R = coordinates of spar endpoints
$z^{sp}(y)$ = z coordinate along spar cap line
$\varepsilon_{xx}, \varepsilon_{yy}, \varepsilon_{zz}, \gamma_{xy}, \gamma_{xz}, \gamma_{yz}$ = engineering strains
$\varepsilon_{\eta\eta}, \gamma_{\eta z}$ = in-plane web strains
$\{\bar{\varepsilon}\}$ = vector of strain components 5×1
η = coordinate along a spar line
Λ = sweep angle of a spar line
ρ = material density
σ_{ij} = stresses
ψ_x, ψ_y = rotations along x and y directions

Introduction

MATHEMATICAL models of wings based on equivalent plate representation combined with global Ritz analysis techniques have been used for basic studies in aeroelasticity and aeroelastic optimization for a long time.[1,2] A structural model based on classical plate theory (CPT) was used in the development of the optimization-driven aeroelastic-tailoring computer capability known as TSO.[3,4] This capability has been extensively tested and widely used for the analysis and preliminary design of wings. Given the simplified nature and limitations of the TSO structural

Received Feb. 19, 1993; revision received Oct. 22, 1993; accepted for publication Oct. 26, 1993.

*Assistant Professor, Department of Aeronautics and Astronautics. Senior Member AIAA.

model compared with the detail and generality of finite element analysis, evaluation of overall accuracy of this equivalent plate structural model for real airplanes such as the YF16 and F15 revealed quite good results.[3,5]

In aeroelastic optimization, some features of equivalent plate wing models are desirable. First, wing geometric definition and structural layout depend on a small number of sizing and shape design variables. As a result, initial model generation and setup is fast compared with the effort needed to generate detailed finite element models. For optimization, this small number of design variables leads naturally to a reduced size design model. Also, assembly of stiffness and mass matrices and solution times for static and dynamic analysis are significantly shorter than those associated with detailed finite element models because of the smaller size of the equivalent plate models. In addition, the global Ritz solution technique, using series of generalized displacement functions that are continuous over the whole planform or over major segments of the wing, makes it possible to obtain structural information at the aerodynamic grid points used in the aerodynamic force computation. Thus, a classical problem of aeroelasticity, the interpolation between the structural and aerodynamic grids, is eliminated.

An important addition to the capabilities of equivalent plate wing structural modeling, the equivalent laminated plate solution (ELAPS) computer code, was introduced by Giles.[6,7] He showed that, using present day computers, a single high-order power series can be used for approximating displacements over wing planforms made of several trapezoidal segments to obtain accurate stress as well as displacement information. The simplicity of manipulating simple power series leads to analytic rather than numerical integration for the mass and stiffness expressions. With the careful organization of computer storage space and order of calculations, major savings in computation times and core storage requirements are achieved. Giles reports CPU times for the polynomial-based equivalent plate technique that are in some cases shorter by an order of magnitude in comparison with corresponding detailed finite element analysis.

ELAPS was used for multidisciplinary structural/aerodynamic optimization of modern wing configurations. A similar structural wing model, in the lifting surface control augmented structural synthesis (LS-CLASS) code,[8,9] adapted for aeroservoelastic applications, made it possible to carry out structural/aerodynamic/control optimization of fiber composite actively controlled wings in an integrated manner.

Equivalent plate wing models bridge the gap between models based on beam theory and detailed finite element models. Although equivalent beam models are still popular for the study of aeroelastic problems and in design, they are limited in their capacity to realistically represent wing structures. In the case of fiber composite wing design, they can even lead to inaccurate results if the effect of the root boundary condition is not taken into account properly.[10,11] Finite element models, such as the ones included in various aeroelastic optimization codes, although general and accurate, can be large and computationally expensive, making them less attractive for preliminary design. If simplified coarse finite element models are used in an effort to speed up computation, then the results might be sensitive to the number and type of elements used as well as the coarseness of the mesh.[12] Methods for combining equivalent plate and finite element structural models have been suggested recently.[13,14] Thus, equivalent plate wing models are important in the context of multidisciplinary wing optimization and wing shape optimization either as independent tools or in combination with finite elements.

However, a recent application to a high-speed civil transport (HSCT) wing[15] exposed some serious limitations of currently used equivalent plate wing models. The plate models used in TSO, ELAPS, and LS-CLASS are all based on the kinematic assumptions of CPT. The extensive studies of Ref. 15 (in which results obtained by the LS-CLASS equivalent plate analysis, Refs. 8 and 9, and the ELFINI finite element structural optimization code, Ref. 16, were compared) revealed that the CPT-based equivalent plate approach led to consistently stiffer models, not being able to capture the coupling between spanwise bending, chordwise bending, and torsion correctly. Chordwise bending due to wing interaction with a flexible fuselage, and some higher modes involving torsional deformations and chordwise deformation, were not predicted properly by the CPT plate model. A careful reexamination of the YF16 test case in Ref. 3 reveals a similar problem with higher mode shapes whose natural frequencies are overpredicted by TSO.

The discrepancies between finite element and CPT-based equivalent plate models appear also in the case of thick high-aspect-ratio wings. One of the test cases in the evaluation of LS-CLASS in Ref. 8 was a high-aspect-ratio thick swept-back wing described in Ref. 17. Static elastic deformations obtained by LS-CLASS with ideal cantilevered boundary conditions were up to about 17% stiffer compared with corresponding finite element results. Natural frequencies, except for first bending, were overpredicted by the equivalent plate model by 35% or more. Again, the largest errors were associated with torsional behavior.

Although using fine-tuned root springs[3,8,18] to impose the boundary conditions improved the plate results for the static case, this had only a limited effect on the natural frequencies.

The YF16 and F15 wings contain several heavy ribs for the transfer of local loads from pylons at external store stations into the wing. Both the HSCT wing and the swept-back wing had only a small number of ribs. In the case of the HSCT wing the webs of these ribs were thin compared with the skin covers. Thus, transverse shear effects due to the internal structure of the wing seem to be important, whereas it is impossible for equivalent plate models based on CPT to capture these effects.

Motivated by the need for reliable and computationally efficient structural modeling for multidisciplinary optimization (including shape optimization) of wings, a new equivalent plate wing modeling capability has been developed and is described in this paper. Key analytical derivations and aspects of numerical implementation are discussed. Behavior sensitivities with respect to wing shape are obtained analytically. The new capability is compared with a CPT-based equivalent plate and to finite element analysis techniques, and its accuracy and reliability are demonstrated.

Wing Geometry and Construction

Depth

A typical wing planform made of three trapezoids is shown in Fig. 1. Depth distribution is defined by specifying the height of each skin cover or spar and rib cap above a reference plane at $z = 0$. A typical height distribution for the ilth layer on the composite skin of a wing section is given by a simple polynomial series

$$z^{il}(x, y) = \sum_{k=1}^{J_h} H_k^{il} \cdot x^{mk} \cdot y^{nk} = h(x, y) \tag{1}$$

The coefficients H_k^{il} can serve as shape design variables. The powers in the series (mk and nk) can be chosen to specify a complete polynomial in x and y or the polynomial obtained by the multiplication of a polynomial in x by a polynomial in y. Different height distributions can be used over the same wing trapezoid to position different composite layers or different spar and rib caps at different

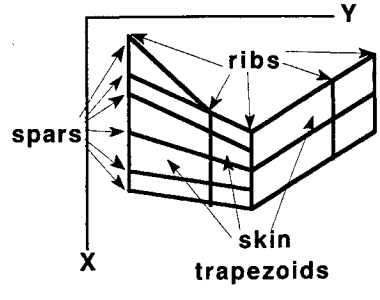

Fig. 1 Skin trapezoids, spar lines, and rib lines on the wing planform.

distances from $z = 0$. Alternatively, just two series can be used for all skin layers and spar and rib caps on one or more trapezoids, lumping them into the upper surface $h_U(x, y)$ and the lower surface $h_L(x, y)$. This is justified when skin thickness is small compared with wing depth. No symmetry with respect to $z = 0$ is assumed. Cutouts, such as due to a wheel bay, can be treated by taking only the upper skin into account.

Construction—Skins, Spars, and Ribs

Upper and lower composite skins can be defined for each planform trapezoid. They are made of layers, each representing plies with a particular fiber direction. The thickness of the ilth layer (ilth fiber direction) on a given trapezoid is specified by a simple polynomial series of the form

$$t^{il}(x, y) = \sum_{j=1}^{J_t} T_j^{il} \cdot x^{mj} y^{nj} \tag{2}$$

The coefficients T_j^{il} can serve as sizing type design variables and the powers (mj and nj) are preassigned. Each spar cap has an area distribution that is linear in y:

$$A(y) = A_1^{sp} y + A_2^{sp} \tag{3}$$

The area A is normal to the spar axis, but rather than expressing it as a function of η, a coordinate along the spar axis, it is expressed in terms of the spanwise coordinate y. This makes it possible to obtain analytical expressions for stiffness and mass contributions of a spar as shown later. Rib cap area is a linear function of x and is defined in the same manner.

Spar webs connect spar caps on the upper and lower wing surfaces that follow the same spar line on the x, y planform. The webs are vertical with respect to the x, y plane (Fig. 2). They are modeled (like the skins) as made of composite layers extending from the lower cap line to the upper cap line and along the spar axis. Thickness of the jlth layer (corresponding to the jlth fiber direction on the web) is given as a function of y

$$t^{jl}(y, z) = T_1^{jl} \cdot y + T_2^{jl} \tag{4}$$

and denotes thickness normal to the plane of the web. Thickness of rib web layers is defined similarly and is linear in the x coordinate.

Construction—Springs and Concentrated Masses

Concentrated linear springs and concentrated masses can be placed at points on the wing structure. Values of the spring coefficients and the concentrated masses can serve as sizing type design variables, whereas the coordinates of their point of attachment can serve as shape design variables. Springs can also be used to represent local stiffness of an attachment between wing segments, such as an aileron and a wing box. They are also useful for boundary conditions in complex configurations. If very stiff springs are chosen, they are used in penalty terms to impose a zero displacement or zero rotation boundary condition. If fine tuned, they can correct for differences between test and experiment by representing actual test support flexibility.[3,8,14,18]

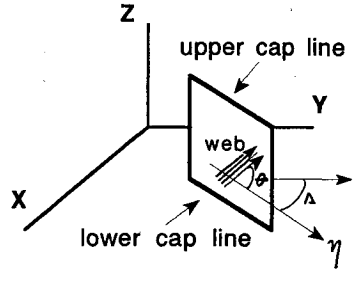

Fig. 2 Spar web and its associated axes.

Planform Geometry

The wing is made of area trapezoids defined by the x and y coordinates of their vertices (Fig. 3). Spar cap lines are defined by x, y coordinates of their endpoints. Ribs are always parallel to the x axis, and their cap lines are defined geometrically by the y coordinate of the rib and the forward and aft x coordinates. The x and y coordinates defining trapezoids, spars, and ribs, as shown in Fig. 3, can serve as planform shape design variables.

Material Properties

Constitutive material matrices for different fiber directions of skin layers are rotated into the x, y system of axes (off axis) so that in the ilth skin layer

$$\begin{Bmatrix} \sigma_{xx} \\ \sigma_{yy} \\ \sigma_{xy} \end{Bmatrix} = [Q^{il}] \begin{Bmatrix} \varepsilon_{xx} \\ \varepsilon_{yy} \\ \gamma_{xy} \end{Bmatrix} \tag{5}$$

For the spar webs (since it is assumed that $\varepsilon_{zz} = 0$, as described in the following), we can write for the jlth layer

$$\begin{Bmatrix} \sigma_{\eta\eta} \\ \sigma_{\eta z} \end{Bmatrix} = [\bar{Q}^{jl}] \begin{Bmatrix} \varepsilon_{\eta\eta} \\ \gamma_{\eta z} \end{Bmatrix} \tag{6}$$

where

$$[\bar{Q}^{jl}] = \begin{bmatrix} Q_{11}^{jl} & Q_{16}^{jl} \\ Q_{61}^{jl} & Q_{66}^{jl} \end{bmatrix} \tag{7}$$

Stiffness of the spar cap is based on its Young's modulus E. Ribs are treated in a similar manner, except that they run in the x direction, and thus their webs are in planes parallel to the xz plane. Density for materials in each skin, spar, and web is also given (ρ).

First-Order Shear Deformation Equivalent Plate Formulation

In an effort to capture transverse shear effects in spar and rib webs, the kinematic assumptions of first-order shear deformation plate theory (FSDPT) are used.[19] The displacements $u, v, w(x, y, z)$ throughout the wing are approximated by

$$\begin{aligned} u(x, y, z, t) &= u_0(x, y, t) + z\psi_x(x, y, t) \\ v(x, y, z, t) &= v_0(x, y, t) + z\psi_y(x, y, t) \\ w(x, y, z, t) &= w_0(x, y, t) \end{aligned} \tag{8}$$

A Ritz approximation method is used in a displacement formulation and the five x, y dependent deformation fields are approximated by

$$\begin{aligned} u_0(x, y, t) &= \{a_1(x, y)\}^T \{q_1(t)\} \\ v_0(x, y, t) &= \{a_2(x, y)\}^T \{q_2(t)\} \\ \psi_x(x, y, t) &= \{a_3(x, y)\}^T \{q_3(t)\} \\ \psi_y(x, y, t) &= \{a_4(x, y)\}^T \{q_4(t)\} \\ w_0(x, y, t) &= \{a_5(x, y)\}^T \{q_5(t)\} \end{aligned} \tag{9}$$

where

$$\{a_r(x, y)\}^T = \{\ldots, x^{mi} y^{ni}, \ldots\} \tag{10}$$

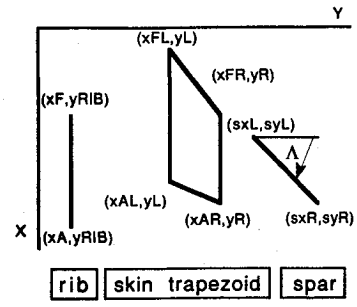

Fig. 3 Planform shape design variables.

That is, simple polynomials are used as shape functions as in Refs. 6–9. The vectors of polynomial terms $\{a_i\}$ can be of different dimensions (and use different series for each of the deformation fields). Thus, the number of terms in each series and the particular powers used (*mi* and *ni*) can vary. However, it is convenient to use the same series in all a_i vectors. If the number of Ritz functions in a series for each $a_i(x, y)$ is n_q, then the total number of degrees of freedom in the problem is $5n_q$.

The fact that deformation field Ritz functions and all depth, layer thickness, and cap area distribution functions are simple polynomials leads to some desirable properties of the formulation as is described in the following sections. However, it also leads to ill conditioning of the stiffness and mass matrices when high-order polynomials are used.

Extensive experimentation[6,8,15] with the use of simple polynomials for CPT-based equivalent plates showed that useful results are obtained before the static solution or eigenvalue solution becomes ill conditioned. In examining the new equivalent plate technique it is important, then, to examine typical convergence properties of the solution in light of this problem.

Mass and Stiffness Matrix Evaluation

All general features of the new formulation can be studied by focusing on mass and stiffness terms arising from skin and spar contributions. Other contributions (from ribs, springs, and concentrated masses) are much simpler to obtain using similar techniques, and thus they are not described here in detail.

Cover Skin Stiffness

We start with the cover skins, assuming that surface curvatures are small and that skin trapezoids are at small angles to the x, y plane. Skins are modeled as thin plane stress panels, in which the engineering strains are

$$\varepsilon_{xx} = \frac{\partial u}{\partial x} = \frac{\partial u_0}{\partial x} + z\frac{\partial \psi_x}{\partial x}$$

$$\varepsilon_{yy} = \frac{\partial v}{\partial y} = \frac{\partial v_0}{\partial y} + z\frac{\partial \psi_y}{\partial y} \tag{11}$$

$$\gamma_{xy} = \frac{\partial u_0}{\partial y} + \frac{\partial v_0}{\partial x} + z\left(\frac{\partial \psi_x}{\partial y} + \frac{\partial \psi_y}{\partial x}\right)$$

Using the Ritz approximations for the five deformation fields [Eqs. (9)] and substituting in Eqs. (11) leads to

$$\begin{Bmatrix} \varepsilon_{xx} \\ \varepsilon_{yy} \\ \gamma_{xy} \end{Bmatrix} = \{ [R_0(x, y)] + z[R_1(x, y)] \}\{q\} \tag{12}$$

$$\{q\}^T = \{q_1^T, q_2^T, q_3^T, q_4^T, q_5^T\} \tag{13}$$

and R_0 and R_1 are $3 \times 5n_q$ matrices partitioned into $1 \times n_q$ subvectors as follows:

$$[R_0(x, y)] = \begin{bmatrix} a_{1,x}^T & 0 & 0\,0\,0 \\ 0 & a_{2,y}^T & 0\,0\,0 \\ a_{1,y}^T & a_{2,x}^T & 0\,0\,0 \end{bmatrix} \tag{14}$$

$$[R_1(x, y)] = \begin{bmatrix} 0\,0\,a_{3,x}^T & 0 & 0 \\ 0\,0\,0 & a_{4,y}^T & 0 \\ 0\,0\,a_{3,y}^T & a_{4,x}^T & 0 \end{bmatrix}$$

where

$$a_{1,x}^T = \frac{\partial \{a_1\}^T}{\partial x} \tag{15}$$

Each element in R_0 and R_1 is the result of differentiation with respect to x or y of a term in the polynomial series for the deformation fields [Eqs. (9) and (10)]. If an original element of any $a_i(x, y)$ is $x^m y^n$, then resulting elements in R_0 and R_1 will be of the forms $mx^{(m-1)}y^n$ or $nx^m y^{(n-1)}$. The general form of elements in R_0 and R_1 is, then, $Cx^i y^j$. R_0 and R_1 are each stored as three matrices: a real $3 \times 5n_q$ matrix containing the coefficients C, an integer matrix containing the powers of x in each term, and another integer matrix containing the powers of y.

The contribution to the strain energy of an area element $dx\,dy$ of the ilth layer (fiber direction) is

$$dU^{il} = \frac{1}{2}\begin{Bmatrix} \varepsilon_{xx} \\ \varepsilon_{yy} \\ \gamma_{xy} \end{Bmatrix}^T [Q]^{il} \begin{Bmatrix} \varepsilon_{xx} \\ \varepsilon_{yy} \\ \gamma_{xy} \end{Bmatrix} t^{il}(x, y)\,dx\,dy \tag{16}$$

Substituting Eq. (12) into Eq. (16), summing up the contributions from all layers il, and integrating over the planform of an area trapezoid result in

$$[K_{\text{skin}}] = \sum_{il} \int_x \int_y t^{il}(x, y)\{R_0^T[Q^{il}]R_0 + z^{il}(R_1^T[Q^{il}]R_0)$$

$$+ z^{il}(R_0^T[Q^{il}]R_1) + (z^{il})^2(R_1^T[Q^{il}]R_1)\}\,dx\,dy \tag{17}$$

Recall that $z^{il}(x, y)$ and $t^{il}(x, y)$ are simple polynomial functions of x and y [Eqs. (1) and (2)]. Each of their elements is also of the form $Cx^i y^j$ (as are the elements of R_0 and R_1) and can also be stored as three vectors: a real vector containing the coefficients and two integer vectors containing the power of x and the power of y of each polynomial term. All elements of the resulting matrix integrand in Eq. (17) are obtained by the multiplication and addition of such polynomial terms, which amounts to matrix multiplications of the coefficients and simple addition of the x powers and the y powers. Each element of the resulting contribution to the stiffness matrix {Eq. (17)} is then a linear combination of area integrals of the form

$$I_{TR}(m, n) = \int_x \int_y x^m y^n\,dx\,dy = \int_{y_L}^{y_R} y^n \cdot \int_{x_F(y)}^{xAy} x^m\,dx\,dy \tag{18}$$

Cover Skin Mass

Substituting Eqs. (9) into Eqs. (8) makes it possible to express the u, v, w components of the deformation in terms of the generalized coordinates $\{q\}$

$$\begin{Bmatrix} u \\ v \\ w \end{Bmatrix} = ([S_0(x,y)] + z[S_1(x,y)])\{q(t)\} \tag{19}$$

where S_0 and S_1 are $3 \times 5n_q$ matrices containing polynomial terms of the form $x^m y^n$. Partitioned into subvectors, they are of the form

$$[S_0(x,y)] = \begin{bmatrix} a_1^T & 0\ 0\ 0 & 0 \\ 0 & a_2^T\ 0\ 0 & 0 \\ 0 & 0\ 0\ 0 & a_5^T \end{bmatrix}$$

$$[S_1(x,y)] = \begin{bmatrix} 0\ 0 & a_3^T & 0\ 0 \\ 0\ 0\ 0 & a_4^T & 0 \\ 0\ 0\ 0 & 0\ 0 & 0 \end{bmatrix} \tag{20}$$

The contribution to the kinetic energy of an infinitesimal skin element $dx\,dy$ of the ilth layer is

$$dT^{il} = \frac{1}{2}\rho_{il} t^{il}(x,y) \begin{Bmatrix} \dot{u} \\ \dot{v} \\ \dot{w} \end{Bmatrix}^T \begin{Bmatrix} \dot{u} \\ \dot{v} \\ \dot{w} \end{Bmatrix} dx\,dy \tag{21}$$

Summing up the contributions from all layers and integrating over the trapezoidal area of a skin segment lead to

$$[M_{\text{skin}}] = \sum_{il} \rho_{il} \int_x \int_y t^{il}(x,y) \times [S_0^T S_0 + z^{il}(S_0^T S_1) + z^{il}(S_1^T S_0) + (z^{il})^2 (S_1^T S_1)]_{(x,y)}\,dx\,dy \tag{22}$$

The result for each mass matrix element is also a linear combination of area integrals of polynomial terms, the same family of area integrals used in the computation of the stiffness terms [Eq. (18)].

Note that global coordinates (x, y) are used throughout the derivation. The wing area trapezoids are not mapped onto unit squares as in Ref. 6. This makes it possible to obtain analytical formulas for stiffness and mass contributions of spars as shown next.

Spar Cap Stiffness

Spar cap lines are defined by the coordinates of their endpoints (y_L, y_R, x_L, x_R) and are generally swept by an angle Λ as shown in Fig. 3. Along the spar line, x is a function of y as follows:

$$x(y) = S_1^P y + S_2^P \tag{23}$$

where

$$S_1^P = \frac{x_R - x_L}{y_R - y_L}$$

$$S_2^P = \frac{x_L y_R - x_R y_L}{y_R - y_L} \tag{24}$$

Normal strain in the cap in terms of strains in global coordinates is given by

$$\varepsilon_{\eta\eta} = \{s^2\Lambda, c^2\Lambda, s\Lambda c\Lambda\} \begin{Bmatrix} \varepsilon_{xx} \\ \varepsilon_{yy} \\ \gamma_{xy} \end{Bmatrix} \tag{25}$$

and the contribution of the cap to the strain energy is

$$U_{\text{sp}}^{\text{cap}} = \frac{1}{2} E \int_0^{Ls} \varepsilon_{\eta\eta}^2 A(\eta)\,d\eta \tag{26}$$

where η is a coordinate along the spar cap line and A is normal to this line. A change of variables from η to y, using

$$d\eta = \frac{dy}{\cos\Lambda} \tag{27}$$

leads to

$$U_{\text{sp}}^{\text{cap}} = \frac{1}{2}\frac{E}{\cos\Lambda} \int_{y_L}^{y_R} \varepsilon_{\eta\eta}^2(x,y)\,A(y)\,dy \tag{28}$$

Substituting Eqs. (12) and (25) into Eq. (28), and defining the vector

$$T_{\text{sp}}^T = \{s^2\Lambda, c^2\Lambda, s\Lambda c\Lambda\} \tag{29}$$

lead to the cap's contribution to the stiffness matrix

$$[K_{\text{sp}}^{\text{cap}}] = \frac{E}{\cos\Lambda} \int_{y_L}^{y_R} [(R_0^T [Q^{\text{sp}}] R_0) + z^{\text{sp}}(R_1^T [Q^{\text{sp}}] R_0) + z^{\text{sp}}(R_0^T [Q^{\text{sp}}] R_1) + (z^{\text{sp}})^2 (R_1^T [Q^{\text{sp}}] R_1)] \cdot (A_1^{\text{sp}} y + A_2^{\text{sp}})\,dy \tag{30}$$

The height of the cap above the reference plane $z = 0$ is given by the height polynomial in x and y Eq. (1) with x replaced by Eq. (23)

$$z^{\text{sp}}(y) = \sum_{k=1}^{J_h} H_k (S_1^P y + S_2^P)^{mk} y^{nk} \tag{31}$$

and the matrix $[Q^{\text{sp}}]$ (3×3) is given by

$$[Q^{\text{sp}}] = \{T_{\text{sp}}\}\{T_{\text{sp}}\}^T \tag{32}$$

As in the case of skin panels, each term of the spar cap stiffness matrix is now made of linear combinations of line integrals of some powers of x and y along the spar line. When x in these integrals is expressed in terms of y [Eq. (23)] and when the integration is carried out with respect to the y coordinate from y_L to y_R, then these line integrals all have the form

$$I_{\text{SP}}(m,n) = \int_{y_L}^{y_R} [x^m(y)]\,y^n dy \tag{33}$$

leading to

$$I_{\text{SP}}(m,n) = \int_{y_L}^{y_R} (S_1^P y + S_2^P)^m y^n dy \tag{34}$$

Spar Cap Contribution to Mass Matrix

The kinetic energy of a spar cap integrated along the line of the spar is

$$T^{\mathrm{sp}} = \frac{1}{2}\frac{\rho^{\mathrm{sp}}}{\cos\Lambda}\int_{y_L}^{y_R} A(y)\begin{Bmatrix}\dot{\bar{u}}\\ \dot{\bar{v}}\\ \dot{\bar{w}}\end{Bmatrix}^T\begin{Bmatrix}\dot{\bar{u}}\\ \dot{\bar{v}}\\ \dot{\bar{w}}\end{Bmatrix}\mathrm{d}y \tag{35}$$

where η has been replaced by y in the integrand. Substituting Eqs. (19) into Eq. (35) leads to

$$[M_{\mathrm{sp}}^{\mathrm{cap}}] = \frac{\rho^{\mathrm{sp}}}{\cos\Lambda}\int_{y_L}^{y_R}[S_0^T S_0 + z^{\mathrm{sp}}(S_0^T S_1)$$

$$+ z^{\mathrm{sp}}(S_1^T S_0) + (z^{\mathrm{sp}})^2(S_1^T S_1)\ ](A_1^{\mathrm{sp}} y + A_2^{\mathrm{sp}})\,\mathrm{d}y \tag{36}$$

When all x powers in the matrices S_0, S_1 are replaced by powers of the spar line equation [Eq. (23)], then it turns out that elements of the spar cap mass matrix are also linear combinations of members of the line integral family in Eq. (34), as are the stiffness terms.

Spar Web Contribution to Stiffness

As shown in Fig. 2, the spar web is normal to the x, y plane and connects two caps running along the same spar line [Eq. (23)] with height above the $z = 0$ plane defined by

$$h_L(x, y) = \sum_{ih=1}^{Ih} H_{ih}^L x^{mih} y^{nih} \tag{37}$$

for the lower cap, and

$$h_U(x, y) = \sum_{jh=1}^{Jh} H_{jh}^U x^{mjh} y^{njh} \tag{38}$$

for the upper cap (*mjh* and *njh* are powers associated with the *jh*th term, etc.).

The web layers are in plane stress. The normal strain in the direction of the spar line and transverse shear strain are obtained from the strains in global coordinates by

$$\varepsilon_{\eta\eta} = \{s^2\Lambda,\ c^2\Lambda,\ s\Lambda c\Lambda\}\begin{Bmatrix}\varepsilon_{xx}\\ \varepsilon_{yy}\\ \gamma_{xy}\end{Bmatrix} \tag{39}$$

and

$$\gamma_{\eta z} = \{s\Lambda,\ c\Lambda\}\begin{Bmatrix}\gamma_{xz}\\ \gamma_{yz}\end{Bmatrix} \tag{40}$$

We define a 2×5 transformation matrix for the web as follows:

$$[T_{25}] = \begin{bmatrix} s^2\Lambda & c^2\Lambda & s\Lambda c\Lambda & 0 & 0\\ 0 & 0 & 0 & s\Lambda & c\Lambda\end{bmatrix} \tag{41}$$

and then

$$\begin{Bmatrix}\varepsilon_{\eta\eta}\\ \gamma_{\eta z}\end{Bmatrix} = [T_{25}]\{\bar{\varepsilon}\} \tag{42}$$

where

$$\{\bar{\varepsilon}\}^T = \{\varepsilon_{xx},\ \varepsilon_{yy},\ \gamma_{xy},\ \gamma_{xz},\ \gamma_{yz}\} \tag{43}$$

The ε_{zz} strain is zero, since the vertical displacement $w(x, y)$ does not depend on z.

Expressing the transverse strains in terms of the unknown deformation fields

$$\gamma_{xz} = \psi_x + \frac{\partial w_0}{\partial x}$$

$$\gamma_{yz} = \psi_y + \frac{\partial w_0}{\partial y} \tag{44}$$

and using Eqs. (9) make it possible to express $\{\bar{\varepsilon}\}$ in terms of the generalized coordinates as follows:

$$\{\bar{\varepsilon}\} = \{\,[W_0] + z[W_1]\,\}\{q\} \tag{45}$$

where the matrices $W_0(x, y)$ and $W_1(x, y)(5 \times 5n_q)$ are partitioned into subvectors and given by

$$[W_0] = \begin{bmatrix} a_{1,x}^T & 0 & 0 & 0 & 0\\ 0 & a_{2,y}^T & 0 & 0 & 0\\ a_{1,y}^T & a_{2,x}^T & 0 & 0 & 0\\ 0 & 0 & a_3^T & 0 & a_{5,x}^T\\ 0 & 0 & 0 & a_4^T & a_{5,y}^T\end{bmatrix}$$

$$[W_1] = \begin{bmatrix} 0 & 0 & a_{3,x}^T & 0 & 0\\ 0 & 0 & 0 & a_{4,y}^T & 0\\ 0 & 0 & a_{3,y}^T & a_{4,x}^T & 0\\ 0 & 0 & 0 & 0 & 0\\ 0 & 0 & 0 & 0 & 0\end{bmatrix} \tag{46}$$

and we define the matrix $(5 \times 5n_q)$

$$[W(x, y, z)] = \{\,[W_0(x, y)] + z[W_1(x, y)]\,\} \tag{47}$$

Now, the contribution to strain energy of an area element $\mathrm{d}\eta\,\mathrm{d}z$ of the *jl*th layer on the web is given by

$$\mathrm{d}U^{jl} = \frac{1}{2}\begin{Bmatrix}\varepsilon_{\eta\eta}\\ \gamma_{\eta z}\end{Bmatrix}^T[\bar{Q}^{jl}]\begin{Bmatrix}\varepsilon_{\eta\eta}\\ \gamma_{\eta z}\end{Bmatrix}t^{jl}(\eta, z)\,\mathrm{d}\eta\,\mathrm{d}z \tag{48}$$

We define

$$[\tilde{Q}^{jl}] = [T_{25}]^T[\bar{Q}^{jl}][T_{25}] \tag{49}$$

and substitute for the layer thickness in terms of y and use

$$\mathrm{d}\eta = \frac{\mathrm{d}y}{\cos\Lambda}$$

This leads to the contribution to the stiffness matrix

$$[K_{\mathrm{web}}^{\mathrm{sp}}]^{jl} = \int_{y_L}^{y_R}\int_{h_L(x,y)}^{h_U(x,y)}(T_1^{jl}\cdot y + T_2^{jl})\,([W(x, y, z)]^T)$$

$$\times\,[\tilde{Q}^{jl}]\,[W(x, y, z)]\,\mathrm{d}z\frac{\mathrm{d}y}{\cos\Lambda} \tag{50}$$

The double integral is integrated analytically first with respect to z, where

$$h_L(x, y) \le z \le h_U(x, y)$$

Equations (37) and (38) are then substituted into

$$\int_{h_L(x,y)}^{h_U(x,y)} z^m \mathrm{d}z = \frac{1}{m+1}\left[h_U^{m+1}(x,y) - h_L^{m+1}(x,y)\right] \tag{51}$$

and all x powers are replaced by powers of

$$x(y) = S_1^P y + S_2^P$$

Each element of the stiffness matrix in Eq. (50) turns out to be a linear combination of the same line integrals of y as those used for the spar cap stiffness and mass [Eq. (34)].

Spar Web Mass Contribution

The contribution of an area element of the jlth layer of the web to the kinetic energy is

$$\mathrm{d}KE^{jl} = \frac{1}{2}\rho^{jl} t^{jl}(y) \begin{Bmatrix} \dot{u} \\ \dot{v} \\ \dot{w} \end{Bmatrix}^T \begin{Bmatrix} \dot{u} \\ \dot{v} \\ \dot{w} \end{Bmatrix} \frac{\mathrm{d}y}{\cos\Lambda}\mathrm{d}z \tag{52}$$

As in the preceding derivations, the substitution of Eqs. (4) and (19), and the integration over the web area over z between $h_L(x,y)$ and $h_U(x,y)$ and along y from y_L to y_R lead to a mass matrix whose elements are, again, linear combinations of the same family of line integrals as the one used for web stiffness and cap stiffness and mass [Eq. (34)].

Thus, all elements of the stiffness and mass matrices due to skins and spars are linear combinations of members of certain families of area and line integrals [Eqs. (18) and (34)]. A similar result is obtained for ribs. This feature of the formulation is important because these area and line integrals can be calculated analytically, and there is no need for numerical integration, as described in the next section.

Area and Line Integrals

The integration in Eq. (18) is carried out analytically first with respect to x between x values on the front line of a trapezoid

$$x_F(y) = F_1 y + F_2 \tag{53}$$

and the aft line

$$x_A(y) = A_1 y + A_2 \tag{54}$$

where F_1, F_2, A_1, and A_2 are determined from coordinates of trapezoidal vertices for the front and aft lines in a manner similar to the coefficients of the spar line in Eqs. (23) and (24). We now define the following two families of line integrals

$$I_F(r,s) = \int_{y_L}^{y_R} y^r (F_1 y + F_2)^s \mathrm{d}y \tag{55}$$

$$I_A(r,s) = \int_{y_L}^{y_R} y^r (A_1 y + A_2)^s \mathrm{d}y \tag{56}$$

so that the area integral [Eq. (18)] over the trapezoid is given in terms of these line integrals by

$$I_{TR}(m,n) = \frac{1}{m+1}\left[I_A(n, m+1) - I_F(n, m+1)\right] \tag{57}$$

Each of these line integrals is obtained analytically by a recursion formula of the form[20]

$$I_F(r,s) = \frac{y_R^{r+1}(F_1 y_R + F_2)^s - y_L^{r+1}(F_1 y_L + F_2)^s}{r+s+1} + \frac{sF_2}{r+s+1}\left[I_F(r, s-1)\right] \tag{58}$$

Note that the same recursion formula applies to the spar line integrals [Eq. (34)], and thus analytical expressions for mass and stiffness matrix elements have been obtained.

Analytical Planform Shape Sensitivities

It was shown in previous sections that all area and line integrals depend in one way or another on a line integral of the form [Eq. (34), (55), and (56)]

$$I_B(r,s) = \int_{y_L}^{y_R} y^r (B_1 y + B_2)^s \mathrm{d}y \tag{59}$$

The coefficients B_1 and B_2 define a straight line in the x, y plane,

$$x(y) = B_1 y + B_2$$

where B_1 and B_2 depend on coordinates of the endpoints of the line, which can serve as planform shape design variables p_i [$B_i = B_i(p_j)$, Eqs. (23) and (24)]. For example, the y coordinate of the left edge y_L can be such a shape design variable. The derivative of the integral I_B with respect to y_L is obtained according to Leibnitz's rule for the differentiation of definite integrals

$$\frac{\partial I_B}{\partial y_L} = \int_{y_L}^{y_R} y^r (B_1 y + B_2)^{s-1} s\left(y\frac{\partial B_1}{\partial y_L} + \frac{\partial B_2}{\partial y_L}\right)\mathrm{d}y - y_L^r (B_1 y_L + B_2)^s \tag{60}$$

or, using Eq. (59),

$$\frac{\partial I_B(r,s)}{\partial y_L} = s\frac{\partial B_2}{\partial y_L} I_B(r, s-1) + s\frac{\partial B_1}{\partial y_L} I_B(r+1, s-1) - y_L^r (B_1 y_L + B_2)^s \tag{61}$$

In these last equations it is assumed that $s \neq 0$. Cases in which $s = 0$, $B_1 = 0$, or $B_2 = 0$ are easier to integrate and the details are not included here.

Examination of Eq. (61) reveals that the shape derivatives of a member of the family of line integrals [Eq. (59)] is a linear combination of other members of the same family plus a term containing powers of y_L, $(B_1 y_L + B_2)$, or y_R, $(B_1 y_R + B_2)$. The same powers are used in the evaluation of the integrals themselves [Eq. (58)] and thus do not have to be evaluated twice.

Shape derivatives of stiffness and mass matrices ($\partial[K]/\partial p$, $\partial[M]/\partial p$, where p is a shape design variable) can then be obtained analytically, leading to analytical derivatives of displacements, stresses, and natural frequencies with respect to shape. Detailed discussion of analytical shape sensitivities in the context of CPT wing equivalent plate modeling can be found in Ref. 22. The extension to FSDPT wing modeling, once $\partial[K]/\partial p$ and $\partial[M]/\partial p$ are available, is straightforward and will not be discussed here. Thus, finite difference derivatives are not needed with the present formulation. In a formulation that tends to be numerically ill conditioned when high-order polynomials are used, finite difference derivatives can lead to large errors if the step size is not

chosen carefully.[21] Using analytical derivatives will save time and be as accurate as the solution itself.[22]

Loads

Two types of static loads are taken into account in the new capability; distributed pressure loads in the z direction, and concentrated forces.

A pressure load is given in simple polynomial form

$$p(x, y) = \sum_l P_l x^{ml} y^{nl} \tag{62}$$

where the coefficients P_l and the powers ml and nl are predetermined. The generalized loads in this case are obtained by integrating the product of pressure and vertical displacement over the planform area. The vertical displacement [Eq. (9)] is also a simple polynomial

$$w(x, y) = \sum_k q_{5_k} x^{mk} y^{nk} \tag{63}$$

The area integration of the product of Eqs. (62) and (63) leads to generalized force terms that, like the skin stiffness and mass contributions, are linear combinations of the area integrals I_{TR} [Eqs. (18)]. This family of integrals is calculated once for the skin trapezoids and then used for stiffness, mass, and load element evaluation as well as all their derivatives with respect to sizing and shape design variables.

Concentrated forces F_k acting in the z direction at points (x_k, y_k) add to the generalized loads associated with the generalized displacement $\{q_5\}$, terms of the form $F_k(x_k)^{mi}(y_k)^{ni}$. Concentrated forces in the x and y directions are treated in a similar manner and affect the generalized loads associated with $\{q_1\}$–$\{q_4\}$. All concentrated force contributions to the static load vector, then, are linear combinations of polynomial terms evaluated at the points of action of these forces. Derivatives with respect to planform shape, if these point of application move due to changes in the planform, are easy to obtain by simple differentiation with respect to x_k and y_k.

Test Case

Application of the new FSDPT equivalent plate technique to a supersonic transport wing is described in Ref. 15. Here the wing of Ref. 17 is used to evaluate the accuracy of the new equivalent plate method. This is an all-aluminum relatively thick wing (21% t/c) of moderate aspect ratio. It is swept back by 30 deg and has an array of spars and ribs as shown in Fig. 4. The wing is cantilevered. Detailed description of the wing as well as experimental measurements of displacements and stresses under load are given in Ref. 17. Finite element modeling accuracy for the static analysis of this wing was studied and reported in Ref. 17, during the early days of the finite element method.

As already described in the Introduction, this wing was used in Ref. 8 as one of the test cases for the evaluation of an equivalent plate wing modeling capability based on CPT. The CPT model was found to be up to 17% too stiff. This was thought to be due to finite flexibility in the test jig used to cantilever the wing and was compensated for by using root springs.[18] Yet, natural frequencies (except for the first bending) were too high and errors were especially large in torsional modes.

Results based on CPT for the test wing are compared here with results from the new FSDPT wing modeling capability, a modern finite element (FE) code (ELFINI[16]), and experiment. The ELFINI finite element model is shown in Fig. 5. It is made of quadrilateral membrane elements for the skin and rod/shear-web elements for the spars and ribs. A 1-lb vertical force applied to the tip of the trailing edge is the static load case considered.

No root springs are used, and in the CPT and FSDPT models, boundary conditions were imposed by proper selection of the Ritz polynomials used to insure zero vertical displacement and zero spanwise rotation at the root.[6,8] The FSDPT and finite element models in this case assume that webs act only in shear.

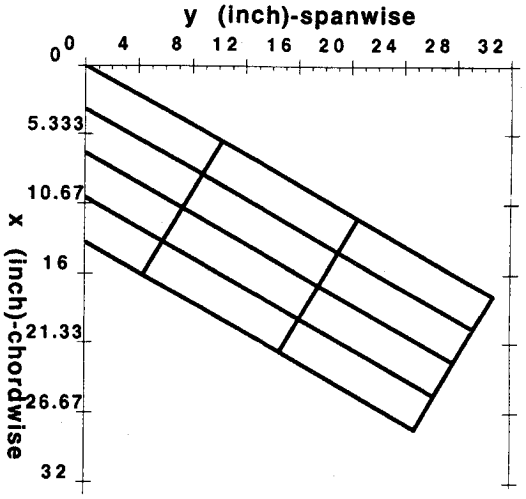

Fig. 4 Planform of the swept-back wing.

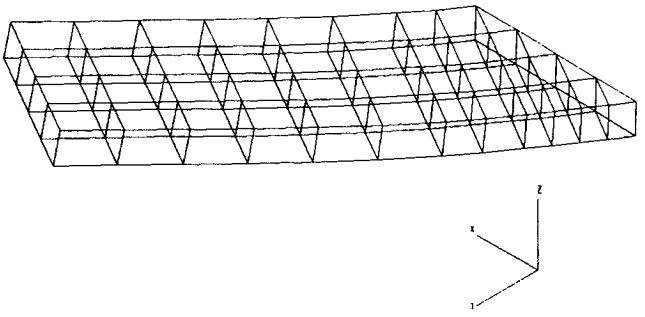

Fig. 5 Finite element model of the swept-back wing.

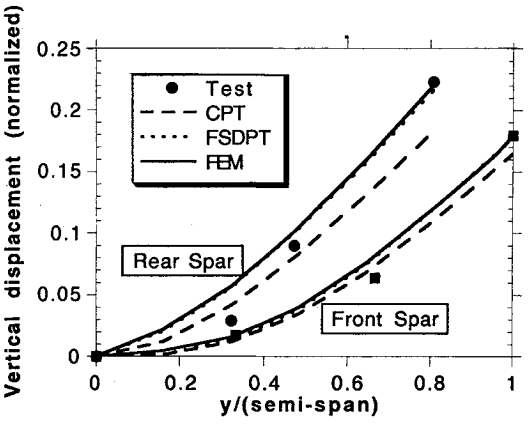

Fig. 6 Calculated and measured static deflections.

Results

Figure 6 shows calculated and measured deflections along the leading edge and trailing edge of the wing. There is an excellent correlation between the new FSDPT equivalent plate model and the finite element results. Good correlation with experiment is obtained for displacements on the outer half of the semispan. The CPT equivalent plate results are considerably stiffer in both bending and torsion. Table 1 lists the natural frequencies of the wing

Table 1 Natural frequencies of the cantilevered swept-back wing, Hz

No.	FE	FSDPT	CPT	Shape
1	115.6	114.7	126.5	1 Bending
2	317.6	312.4	——	Fore/aft
3	418.4	428.9	606.5	1 Tosion
4	576.4	575.3	797.2	2 Bending
5	1086	1125	1831	2 Torsion

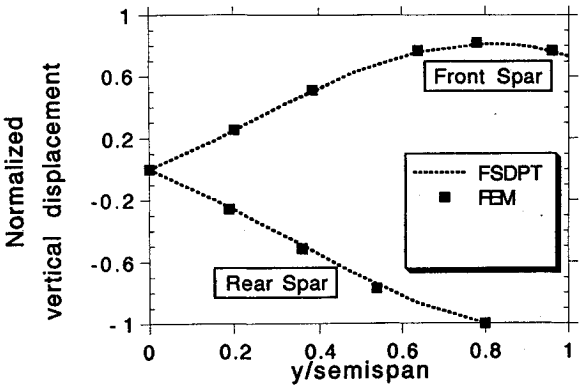

Fig. 7 First torsion mode shape (FEM and FSDPT).

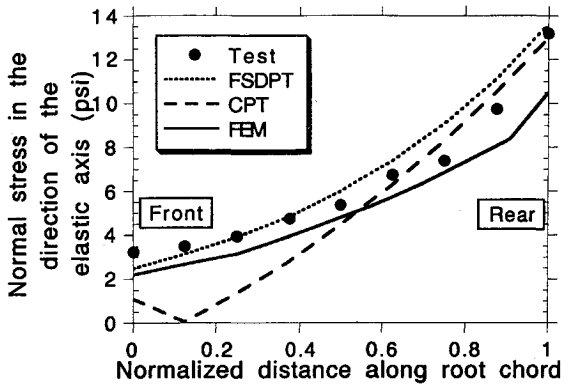

Fig. 8 Skin stress $\sigma_{\eta\eta}$ along the root chord.

based on theoretical structural mass. Whereas the new FSDPT method captures all frequencies and mode shapes in the range shown, including the fore-aft modes, the CPT method leads to large errors in higher natural frequencies, especially those associated with torsional behavior. A comparison of mode shape for the first torsion mode between the finite element and FSDPT results is shown in Fig. 7. The correlation is excellent.

In addition to accurate deformations and mode shapes, reliable stress predictions are important in approximate structural analysis methods, if these methods are to be useful for multidisciplinary optimization. Figure 8 shows normal skin stresses in the directions of the spars η at points along the root chord. The rise in stresses toward the rear point of the root chord (typical in swept-back wings) is captured by all analysis methods. The discrepancy in the finite element results is probably due to a mesh that is too coarse at the stress concentration area at the root. Both plate models, based on polynomial approximation, capture the stresses in the stress concentration area quite well (with polynomials of the order 7 for CPT and order 5 for FSDPT). Stresses toward the leading edge of the root chord are predicted reasonably well by the finite element and FSDPT models, whereas the CPT model leads to large discrepancies in the front end of the root chord. Normal skin stresses

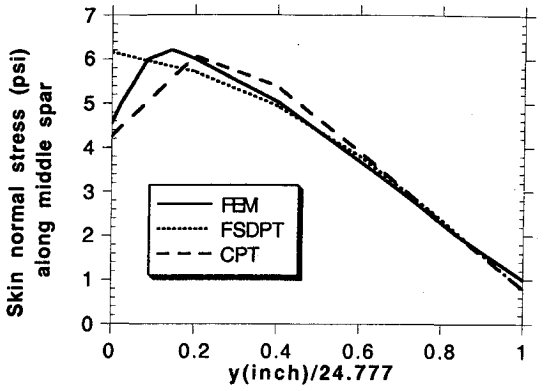

Fig. 9 Skin stress $\sigma_{\eta\eta}$ along the middle spar line.

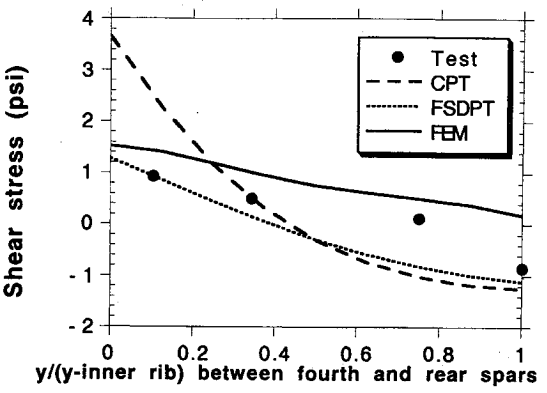

Fig. 10 Skin shear stresses $\tau_{\zeta\eta}$ the along a line between the fourth and rear spars (from root to inner rib).

in the spar direction η along the middle spar line are shown in Fig. 9. Except for differences at the root region (already shown in Fig. 8), results from the finite element, CPT, and FSDPT plate models correlate well.

A harder task, in the case of the swept-back wing, is the evaluation of skin shear stresses and normal stresses perpendicular to the spar lines. These stresses are small compared with the normal stresses in the spar direction. Errors in their measured values can be large.[17]

Figure 10 shows skin shear stresses between the root and inner rib, along a line between the fourth and fifth (rear) wing spars. Experimental values fall between results from the finite element and FSDPT models. The CPT model, however, overpredicts these stresses in the root region near the stress concentration. Comparison of shear stresses away from the stress concentration, along a line between the first (leading edge) and second spars from root to inboard rib, is shown in Fig. 11. There are differences between the various analysis methods and test results (test results for skin shear stresses near the rib are questionable, as pointed out in Ref. 17). Overall these stresses are small compared with the normal stresses, and their order of magnitude is correctly predicted by all three analysis methods.

Convergence histories of typical displacement, natural frequency, and stress predictions are shown in Fig. 12. Recall that both CPT and FSDPT equivalent plate techniques here are based on simple polynomials as Ritz functions, leading to ill conditioning of the static and eigenvalue solutions as the order of these polynomials goes up. Thus, convergence of results cannot be guaranteed. The experience of Refs. 6–8 was that useful results could be obtained before this ill conditioning became too severe. Indeed, Fig. 12 shows that differences in displacement and natural frequency predictions change by less than 2% when polynomial order

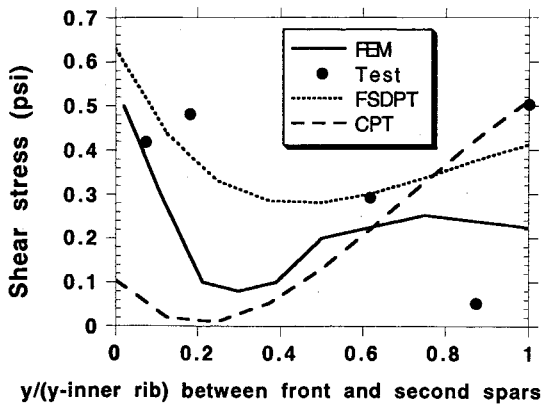

Fig. 11 Skin shear stresses $\tau_{\zeta\eta}$ the along a line between the front and second spars (from root to inner rib).

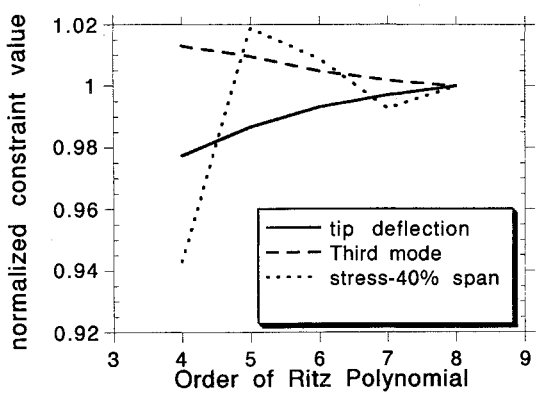

Fig. 12 Convergence of typical displacement, stress, and natural frequency predictions.

is increased from 5 to 8. Stress predictions are slower to converge, as expected, and oscillate. However, their variation, as the order of Ritz polynomials increases, is also smaller than 2%.

Computational Efficiency

A computational advantage of the two equivalent plate techniques over standard finite element techniques is due to the smaller size of the resulting mass and stiffness matrices. Some other computational considerations in the present formulation (such as generating the required families of integrals and polynomial powers, to be later used for stiffness, mass, load elements, and analytical sensitivities) have already been discussed. Another technique for accelerating computation is replacing the spar and rib webs by an equivalent sandwich core.[23] Spar and rib webs are similar to skin panels and computation of their contribution to stiffness and mass can be time consuming. In a wing with many spars or ribs,[15] this requires considerable computational resources. If an array of many spars and ribs is replaced by a core of given distributed stiffness, the core contribution is evaluated once in terms of area integrals [Eq. (18)], and the repeated evaluation of spar and rib web stiffness and mass is not required. A detailed discussion of equivalent core formulations is beyond the scope of this paper.

Conclusion

Limitations of CPT-based equivalent plate structural modeling techniques were described for cases involving thin spar/rib webs (or small numbers of ribs) in low-aspect-ratio wings or thick high-aspect-ratio wings. A new wing equivalent plate modeling technique based on first-order shear deformation plate theory has been presented. Analytical and computational aspects of the new capability were discussed. Detailed derivation of analytical expressions for stiffness and mass contributions from composite skins and spars were used to expose all of the main features of the new capability, including analytical sensitivities with respect to planform shape. Application to a case of a thick swept-back wing showed that the new capability performs as well as corresponding finite element analysis and correlates well with experiment.

Equivalent plate structural wing modeling techniques are important in the context of preliminary design and multidisciplinary optimization. The new capability adds to the reliability and generality of these techniques.

Acknowledgments

This research was partially supported by NASA. Hiro Miura of NASA Ames Research Center was the technical monitor, and his support, encouragement, and willingness to share his experience are greatly appreciated. The author thanks Gary Giles of NASA Langley Research Center for many helpful discussions. Kumar G. Bhatia and Robert A. Sels from Boeing helped with advice and finite element modeling. Their support was instrumental to the completion of this work.

References

[1]Schmit, L. A., and Balmer, H.A., "Procedures for Including Temperature Effects in Structural Analysis of Elastic Wings," Wright Air Development Center, WADC TR 57-754, NTIS AD 230 981, Dayton, OH, May 1959.

[2]Miura, H., "An Optimal Configuration Design of Lifting Surface Type Structures under Dynamic Constraints," Ph.D. Thesis, Case Western Reserve Univ., Cleveland, OH, Jan. 1972.

[3]Lynch, R. W., Rogers, W. A., and Brayman, W. W., "Aeroelastic Tailoring of Advanced Composite Structures for Military Aircraft," U.S. Air Force Flight Dynamics Lab, AFFDL-TR-76-100, Dayton, OH, April 1977.

[4]McCullers, L.A., "Automated Design of Advanced Composite Structures," *Mechanics of Composite Materials*, edited by Z. Hashin, Pergamon Press, Oxford, England, UK, 1983.

[5]Triplett, W. E., "Aeroelastic Tailoring Studies in Fighter Aircraft Design," *Journal of Aircraft*, Vol. 17, No. 7, 1980, pp. 508–513.

[6]Giles, G. L., "Equivalent Plate Analysis of Aircraft Wing Box Structures with General Planform Geometry," *Journal of Aircraft*, Vol. 23, No. 11, 1986, pp. 859–864.

[7]Giles, G. L., "Further Generalization of an Equivalent Plate Representation for Aircraft Structural Analysis," *Journal of Aircraft*, Vol. 26, No. 1, 1989, pp. 67–74.

[8]Livne, E., Schmit, L. A., and Friedmann, P. P., "Design Oriented Structural Analysis for Fiber Composite Wings," Dept. of Mechanical, Aerospace, and Nuclear Engineering, Univ. of California, Los Angeles, UCLA-ENG-88-36, Los Angeles, Los Angeles, CA, Nov. 1988.

[9]Livne, E., "Integrated Multidisciplinary Optimization of Actively Controlled Fiber Composite Wings," Ph.D. Dissertation, Mechanical, Aerospace, and Nuclear Engineering Dept., Univ. of California, Los Angeles, Los Angeles, CA, 1990.

[10]Librescu, L., and Simovich, J., "A General Formulation for the Aeroelastic Divergence of Composite Sweptforward Wing Structures," *Journal of Aircraft*, Vol. 25, No. 4, 1988, pp. 364–371

[11]Lottati, I., "Flutter and Divergence Aeroelastic Characteristics for Composite Forward Swept Cantilevered Wing," *Journal of Aircraft*, Vol. 22, No. 11, 1985, pp. 1001–1007.

[12]Striz, A. G., and Venkayya, V. B., "Influence of Structural and Aerodynamic Modeling on Flutter Analysis," *Proceedings of the AIAA/ASME/ASCE/AHS/ASC 31st Structures, Structural Dynamics, and Materials Conference*, Pt. 1, AIAA, Washington, DC, 1990, pp. 110–118.

[13]Chang, K. J., Haftka, R.T., Giles, G.L., and Kao, P.J., "Sensitivity Based Scaling for Correlating Structural Response from Different Analytical Models," *Proceedings of the AIAA/ASME/ASCE/AHS/ASC 32nd Structures, Structural Dynamics, and Materials Conference*, Pt. 1, AIAA, Washington, DC, 1991, pp. 238–246 (AIAA Paper 91-0925).

[14]Kao, P. J., "Coupled Raleigh-Ritz/Finite Element Structural Analysis using Penalty Function Method," *Proceedings of the AIAA/ASME/ASCE/AHS/ASC 33rd Structures, Structural Dynamics, and Materials Conference* (Dallas, TX), Pt. 1, AIAA, Washington, DC, 1992, pp. 135–141 (AIAA Paper 92-2238).

[15]Livne, E., Sels, R. A., and Bhatia, K. G., "Lessons Learned from Application of Equivalent Plate Structural Modeling to an HSCT Wing," *Proceedings of the AIAA/ASME/ASCE/AHS/ASC 34th Structures, Structural*

Dynamics, and Materials Conference, Pt. 2, AIAA, Washington, DC, pp. 959–969 (AIAA Paper 93-1413).

[16]Lecina, G., and Petiau, C., "Advances in Optimal Design with Composite Materials," *Computer Aided Optimal Design: Structural and Mechanical Systems*, edited by C. A. Mota-Soares, Springer-Verlag, Berlin, 1987.

[17]Turner, M. J., Martin, H. C., and Weikel, R. C., "Further Development and Application of the Stiffness Method," *Matrix Methods of Structural Analysis*, edited by F. B. de Veubeker, Pergamon, Oxford, England, UK, 1964, pp. 203–266.

[18]Gallagher, R. H., and Rattinger, I., "The Deformational Behavior of Low Aspect Ratio Multi Web Wings", *The Aeronautical Quarterly*, Nov. 1961, pp. 361–371, Feb. 1962, pp. 71–87, May 1962, pp. 143–166; also in *A Correlation Study of Methods of Matrix Structural Analysis*, Macmillan, New York, 1964.

[19]Reddy, J. N., *Energy and Variational Methods in Applied Mechanics*, Wiley, New York, 1984, Chap. 4

[20]Spiegel, M. R., *Mathematical Handbook*, Schaum's Outline Series, McGraw-Hill, New York, 1968.

[21]Haftka, R. T., and Gurdal, Z., "Elements of Structural Optimization," 3rd ed., Kluwer, Dordrecht, The Netherlands, 1992, pp. 256–263.

[22]Livne, E., "Analytical Sensitivities for Shape Optimization in Equivalent Plate Structural Wing Models," *Journal of Aircraft* (to be published).

[23]Jeon, J. S., and Hong, C. S., "Bending of Tapered Anisotropic Plates with Arbitrary Edge Conditions," *AIAA Journal*, Vol. 30, No. 7, 1992, pp. 1762–1769.